Impact of magnetic, thermal, structural, morphological and optical characteristics on room temperature ferromagnetism of pristine and cerium doped ZnO nanocomposites

P. Kanakarajan[a*], P. Gopinath[b], S. Krishnakumar[c], P.M.Vivek [d]
[a*,b]*Department of Mechanical Engineering, K.S.R.College of Engineering, Tiruchengode – 637215*
[c]*Assistant Professor, Department of Mechanical Engineering, Gnanamani College of Technology, Pachal, Namakkal - 637 018*
[d]*Assistant Professor, Department of Chemistry, Vel Tech Rangarajan Dr. Sagunthala R&D Institute of Science and Technology (Deemed University), Avadi-600 062, Chennai, Tamil Nadu, India.*

An excellent fit between the theoretical and experimental studies of the related to structure, optics, and magnetism features of pristine and cerium-modified Zn-O NPs prepared through the wet chemical technique. Refining the XR-D pattern using the Rietveld-method reveals that the samples have a hexagonal Wurtzite structure. Absorption spectra reveal a shrinking bandwidth gap as cerium doping increases, substantiating ce^{2+} ion's essential function in ZnO's spectral qualities. The narrowing of the bandwidth gap due to the presence of impurity states was also verified by first-principles calculations. The residual magnetization increases with Cerium doping, and magnetic tests show room-temperature weak-ferromagnetism (RTFM). In addition, ferromagnetism for cerium doping is confirmed by both first-principles calculations and experiments. Theoretical calculations imply that the cerium atoms may agglomerate to generate metallic-antiferromagnetic chromium oxide when cerium doping reaches 8%. At ambient temperature, however, ferromagnetic behaviour is feasible since both ferromagnetic and antiferromagnetic behaviour are degraded when cerium is widely disseminated throughout the lattice as revealed by XRD studies.

(Received September 20, 2023; Accepted June 12, 2024)

Keywords: Mechanical, Magnetic, Thermal, VSM, RTFM

1. Introduction

Diluted attracting oxides have sparked significant interest over the last two decades due to their intricate physics and promising prospects in the field of spintronics[1]. The discovery of ferromagnetism in metallic materials has spurred the quest to seek appropriate substances for spintronics devices that can function at ambient temperatures[2]. Dietl made a prediction on the potential for transition metal-doped ZnO to have Curie temperatures that surpass the ambient room temperature[3]. Following that, there have been reports of ferromagnetism at room temperature in ZnO that has been doped with different metals. The contentious nature surrounding the source of ferromagnetism at ambient temperature in these systems remains unresolved[4]. There is ongoing discussion over the underlying cause of the observed phenomenon, with differing viewpoints attributing it to inherent factors, flaws, or clustering of the magnetic ions[5]. In order to address the uncertainty around the intrinsic or extrinsic nature of ferromagnetism, an endeavour is being made to introduce nonmagnetic ions into ZnO via a process known as doping[6]. The precise source of room temperature ferromagnetism remains uncertain; nonetheless, it is evident that some exchange process must be accountable for the establishment of ferromagnetic ordering in Diluted magnetic oxides[7]. The prevailing antiferromagnetic and short-range superexchange mechanism fails to account for the occurrence of ferromagnetic ordering below the percolation threshold of

* Corresponding author: saravananphd2022@gmail.com
https://doi.org/10.15251/DJNB.2024.192.933

19.8% in hexagonal wurtzite ZnO[8]. There is a prevalent consensus in the scientific literature that the phenomenon of room temperature ferromagnetism may be seen in doped ZnO, even when the dopant concentration is quite low. The phenomenon of ferromagnetic double exchange is capable of generating a significant magnetic moment, however it is characterised by a limited range of interaction. This study presents an investigation of the optical and magnetic characteristics of undoped ZnO and Cerium-doped ZnO samples, which were synthesised using a wet chemical process[9,10]. In this work, the incorporation of Cerium into the ZnO lattice is used as a means to modify its characteristics, including its structural, optical, and room temperature ferromagnetic properties. The discussion also included the investigation of the source of ferromagnetic ordering at room temperature (RT) and the inherent defect in the manufactured samples of pure and cerium-doped ZnO nanoparticles. According to the available studies, it can be inferred that this material has favourable characteristics for a wide range of applications in electromagnetic devices.

2. Experimental methodology

Using methyl cellosolve as a stabiliser, samples of ZnO and ZnO with cerium doping were generated by the wet chemical technique. The reactants, a solvent, and stabiliser in this procedure were zinc-nitrate hexahydrate, methyl cellosolve, and Triethanolamine (TEA), respectively. Sol-gel samples of Pure and cerium-doped ZnO were made by adding methyl cellosolve as a stabiliser. After being stirred with a magnetic stirrer at 60°C during the night, the resultant solution was stable and homogenous, with no visible particles or precipitates. After 24 hours of drying at 100 degrees Celsius, the resulting solution was crushed into powder. After it dried, the gel was fired up for 2 hours at 450 degrees Celsius. The samples were then pressed into pellet and heated at 500 degrees Celsius.

3. Result and discussion

3.1. Crystal Structure and Crystallite Studies

The patterns determined by XRD of both undoped ZnO and Ce-ZnO are shown in Figure 1. The peak values for diffraction are consistent with the conventional JCPDS cards (36-1451), which have a hexagonal wurtzite structure ZnO as their basis[11]. By using the least squares approach to fit the XRD data, the lattice parameters of these samples are calculated and shown in Table 1. Ce-ZnO is discovered to have somewhat higher lattice parameters compared to undoped ZnO. Due to the substantial ionic radius difference between Zn^{2+} and doped ions, the enhanced lattice characteristics suggest that the co-doped ions of Ce^{2+} may be doped into the ZnO crystal lattice by replacement of the Zn^{2+} sites. Scherrer's formula is used to determine the mean size[12],

$$D = 0.89\lambda/\beta Cos\,\theta \quad (1)$$

In the given context, λ represents the X-ray wavelength, β denotes the whole width at half maximum, and θ signifies the maximum of the Bragg diffraction peak. According to the data shown in Table 1, the mean dimensions of the synthesised pure and cerium-doped ZnO nanoparticles, specifically for the (101), are around 32 nm and 17 nm, correspondingly.

$$\beta\, Cos\,\theta = k\lambda/D + 4\varepsilon\, sin\,\theta \quad (2)$$

The constant K is dependent on the form of the crystallite, while λ represents the wavelength of the X-rays used in the diffraction process. Additionally, D denotes the diameter of the crystallite, while ε signifies the strain present inside the crystal. The estimation of the interplanar distance (d-spacing) of a cubic lattice was conducted using Bragg's diffraction equation: 2dsin θ = n λ, where n represents an integer value of 1. The lattice parameter (a) of a cubic unit cell was calculated using the given relation.

$$d = a/\sqrt{h2 + k2 + l2} \quad (3)$$

The variable "d" represents the d-spacing, whereas "h," "k," and "l" denote the Miller indices. The d-spacing and lattice parameter were recorded and shown in Table 1.

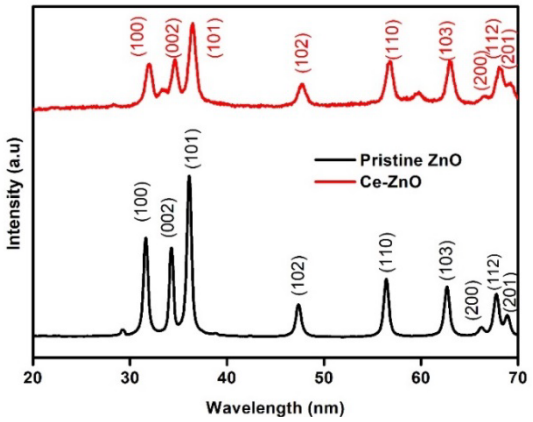

Fig. 1. XRD analysis of Pristine and Cerium incorporated Zinc Oxide.

Table 1. The results obtained from XRD analysis.

Samples	A(Å)	D spacing(Å)	C(Å)	Average size(nm)
ZnO	3.27	2.31	5.281	32
Ce-ZnO	3.30	2.35	5.396	17

3.2. Surface Morphology studies

Figure 2a&b illustrates the reduction in size of Pristine and Cerium doped ZnO may be further substantiated via the use of transmission electron microscopy (TEM) photographs.

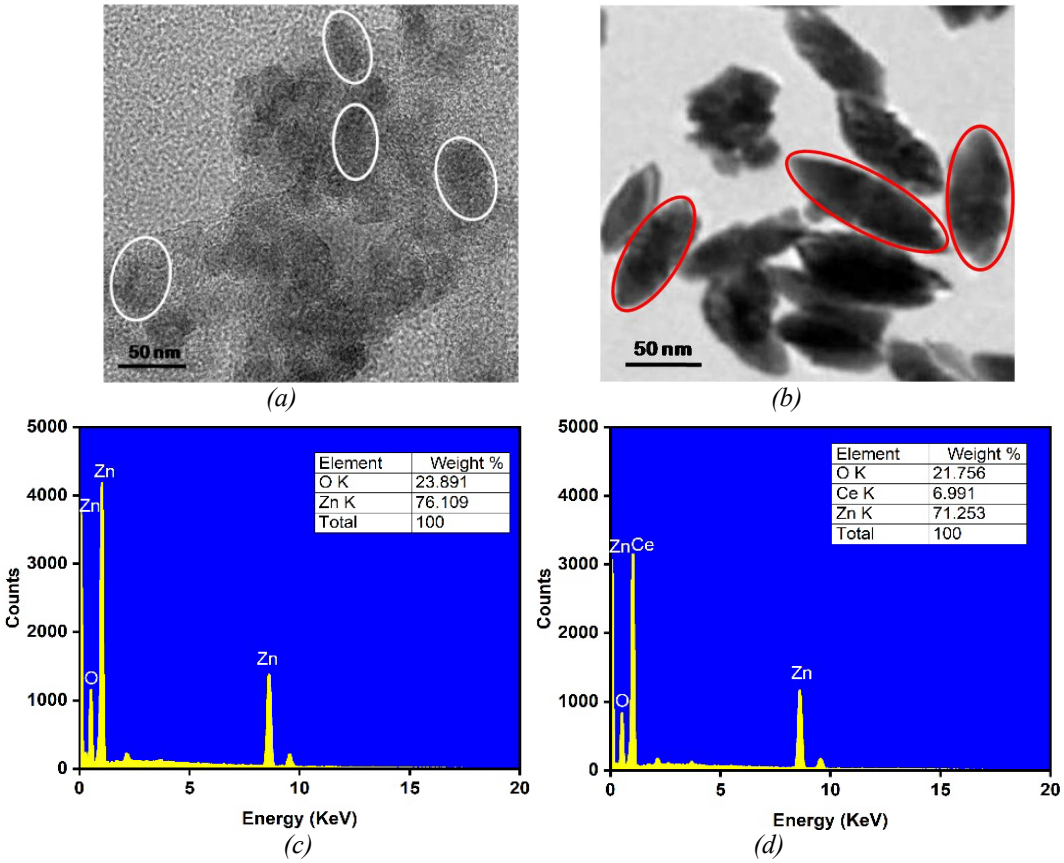

Fig. 2. (a and b) TEM analysis c&d) EDAX analysis of Pristine and Cerium incorporated Zinc Oxide.

The transmission electron microscopy (TEM) picture of synthesized materials displays spherical particles with an average diameter of 23 nm, as shown in Figure 2 (a). In contrast to pristine ZnO, changes in the quantities of doping ions (Cu^{2+}) do not result in significant modifications to the shape of the nanoparticle. The average particle size of ZnO samples shows a drop from 23 to 14 nm when the doping with Ce^{2+} are altered, hence displaying a favourable correspondence with the XRD data. The mean size of the particles found in these specimens exhibits a reduction when the amounts of doping ions (Ce^{2+}) fluctuate. This phenomenon may be ascribed to the interference of the doping ions with the formation of the ZnO crystal[13].

3.3. FTIR analysis

The KBr technique measured the distinctive peaks of samples 500 and 3500 cm^{-1} at room temperature, as shown in Fig. 3. O-H stretching vibration in the nanocrystalline of ZnO is responsible for the peaks at 3592 cm^{-1} and 3369 cm^{-1}. The peak of absorption around 2119 cm^{-1} for pure and 2047 cm^{-1} for Ce doped ZnO may be attributed to atmospheric carbondioxide molecules. Below 1010 cm^{-1} in FTIR spectra, functional groups and Zn-O & Ce-O bonds may be shown to exist or not. Absorption wavelengths from 732 and 836 cm^{-1} demonstrate the evolution of the microstructure as a result of Ce doping. The defect density surrounding Ce ions in the ZnO network manifests as a noticeable and highly strong absorption peak in the Ce doped material. Absorption peak at 562 cm^{-1} have been linked to the stretching mode of Zn-O bonding in pure ZnO. Absorption peaks for a Ce doped sample range from around 496 cm^{-1} to about 580 cm^{-1} due to the distortion created by the initial doping of Ce into Zn-O[14]. More Ce doping shifts the absorption peaks towards the low wave number end of the spectra due to the difference in bond length between Ce^{2+} ions and Zn ions. An O-H stretching mode bonded to hydrogen causes a peak at 3592 cm^{-1}, 3369 cm^{-1}, and 2968 cm^{-1} in both undoped and doped ZnO NPs. There are peaks at 1452 cm^{-1}, 2047 cm^{-1}, and 1456 cm^{-1}, which correspond to the C=O stretching bending vibrations.

One can see the bond peak at 562 cm^{-1}, and 642 cm^{-1} in ZnO, which represents the vibration associated with the stretching mode.

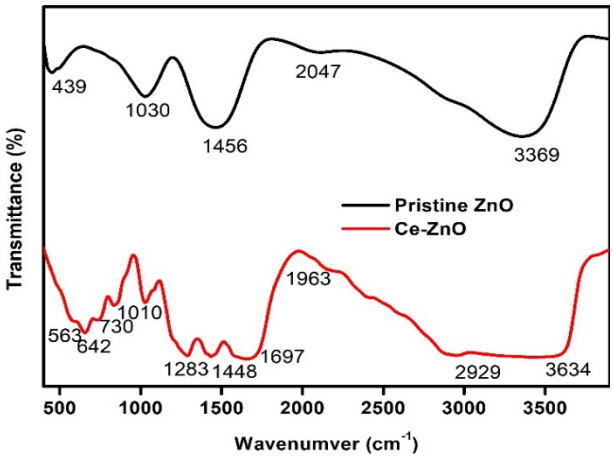

Fig. 3. FTIR analysis of a) Pristine and b) Cerium incorporated Zinc Oxide.

3.4. Photoluminescence Analysis

The luminescent spectra of both pure ZnO and Ce doped ZnO materials are shown in Figure 4. 4 peaks may be seen in the spectrum, much as in the luminescent spectra of pure ZnO materials. The first pair of peaks, at 361 nm and 384 nm, are the result of electrons in conduction band and holes in valence band replication, while the peak levels at 465 nm and 534 nm are the consequence of electron and holes interaction[15]. Ce^{2+} have been injected into the ZnO system as seen by the intensity change, and the broad peaks show that fewer defects exist in the produced Cerium doped ZnO NPs.

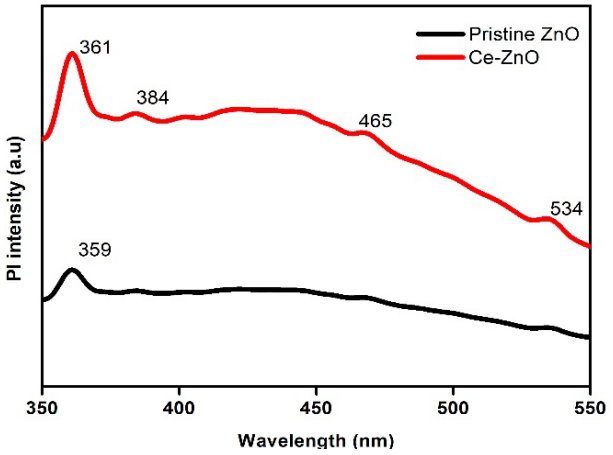

Fig. 4. PL analysis of a) Pristine and b) Cerium incorporated Zinc Oxide.

3.5. Thermal Analysis

During the manufacturing of ZnO and Ce-ZnO nanoparticles, differential thermal analysis and thermo gravimetric analysis (DTA/TGA) were carried out. During the synthesis process, approximately forty percent of the sample's initial weight is lost as a result of the removal and decomposition of organic groups that were present in the sample prior to the beginning of the process (as depicted by the TGA curve in Figure 5). This weight loss is caused by the evaporation of water, which begins at about two hundred degrees Celsius and peaks between three hundred and

fifty and four hundred and fifty degrees Celsius for both pure zinc oxide and cerium zinc oxide. Above 750 degrees Celsius, there is neither a breakdown nor a reaction that may take place. The DTA curve shown in Figure 5 between 200 and 600 degrees Celsius shows maximums for both samples at 400 degrees Celsius. This peak in exothermic activity represents the combustion of organic material. Nevertheless, no further exothermic nor endothermic peaks are seen in the DTA plot.

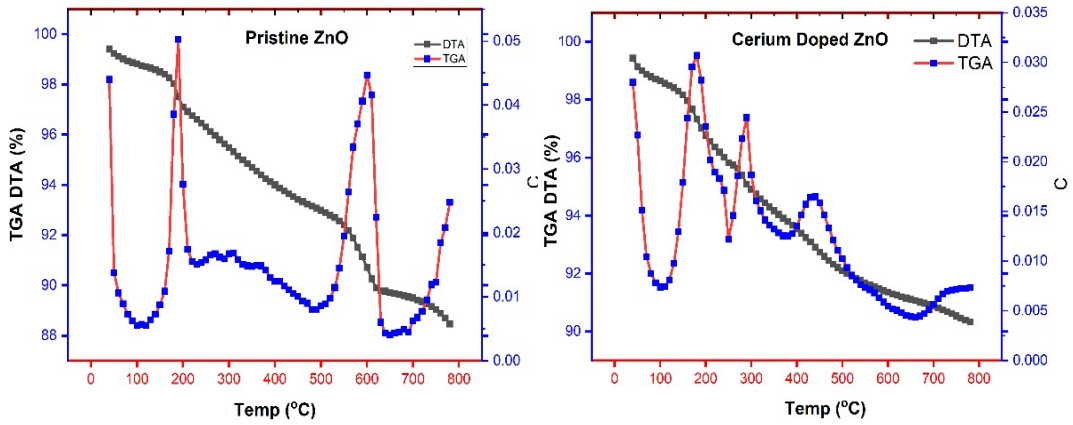

Fig. 5. Thermal analysis of Pristine and Cerium incorporated Zinc Oxide.

3.6. VSM Analysis

The ZnO and Ce-ZnO nanocomposites were tested for their M-H hysteresis loops at ambient temperature, and the outcomes are shown in the figure 6. ZnO and Ce-ZnO possess distinct M-H hysteresis loops. The magnetization properties of the produced nano nanocomposite are shown clearly in the image. Optimal magnetism for the nanocomposite samples is 13.81 emu/g and 6.91 emu/ g, whereas the coercive force is 129 Oe and 69 Oe. In contrast to doped samples, the saturation magnetization of nanocomposite samples rises as ZnO doping. Both intrinsic magnetism (arising from exchange interactions) and extrinsic magnetism (including the creation of secondary phase elements) may account for the magnetism of NPs at ambient temperature[16]. The X-ray diffraction pattern reveals that there are no secondary or impurity phases. The EDAX analysis also shows that the analysed samples contain no additional elements. According to the data presented above, the creation of clusters of transition elements is responsible for the occurrence of the room temperature, and no secondary phase elements have been detected in the produced samples. Therefore, ferromagnetism at ambient temperature produced using undoped ZnO, Ce-ZnO nanocomposites is an inherent magnetic feature of these materials. The XRD analysis clearly demonstrates that Ce has been integrated into the ZnO lattice. Magnetism in nanocomposites is thought to originate via exchange contact between local spin polarised electrons and the conductive electrons, as a result of the introduction of Ce^{2+} ions into the ZnO lattice. At room temperature, VSM measurements of the ferromagnetic characteristics of the Ce doped ZnO NPs yielded the findings shown in the figure. It is the kind and density of magnetic carriers that determine the ferromagnetic ordering in ZnO-based DMS materials. Ce doped ZnO NPs samples were tested for their magnetic characteristics, and the results are listed below. Increasing the Ce doping ratio is found to boost the resulting coercivity value.

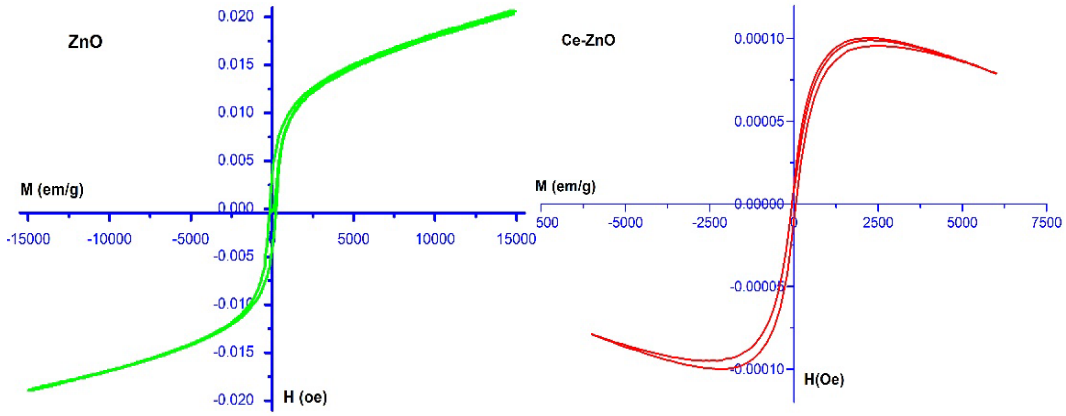

Fig. 6. VSM analysis of a) Pristine and b) Cerium incorporated Zinc Oxide.

Table 2. Properties of synthesized materials.

Properties	Ce-ZnO	Pristine ZnO
Coercivity (Oe)	129	69
Saturation Magnetization ($x10^{-3}$ emu/g)	10.823	13.754
Remanent Magnetization ($x10^{-3}$ emu/g)	1.78	4.31
Percentage remanence (%)	15%	29%

4. Conclusion

Pristine zinc oxide and cerium-doped zinc oxide nanoparticles with controllable size were synthesised using a novel wet chemical technique. The X-ray diffraction analyses indicated that the nanoparticles that were synthesised exhibited a hexagonal wurzite crystal structure. X-ray diffraction investigations indicate the presence of nanoparticles with average dimensions of 23 nm and 11 nm, respectively. Fourier Transform Infrared spectroscopy was used to validate the presence of functional groups in the synthesised nanoparticles. The TEM picture revealed that the synthesised nanoparticles exhibited elongated spherical and capsule-like morphologies. The hysteresis loop discovered in the VSM tests indicates the presence of ferromagnetic properties at ambient temperature. The determination of the coercivity value of the synthesised nanoparticles provided evidence for the presence of a soft ferromagnetic substance. The nanoparticles investigated in this investigation, both undoped and Ce-doped, exhibit low magnetism. These nanoparticles have the potential to function as diluted magnetic-semiconductors, making them suitable for spintronic applications.

References

[1] Mak, Kin Fai, Jie Shan, Daniel C. Ralph, Nature Reviews Physics 1, no. 11 (2019): 646-661; https://doi.org/10.1038/s42254-019-0110-y

[2] Sathya, V., Jagatheesan, R., Jeevanantham, V., Gopi, D., & Baby Shakila, P. Journal of Applied Electrochemistry, 53 no 9, (2023)1887-1894. https://doi.org/10.1007/s13399-023-04793-7

[3] Ren, Hongtao, Gang Xiang, Nanomaterials 11, no. 12 (2021): 3199; https://doi.org/10.3390/nano11123199

[4] Jagadeeswari, R., Selvakumar, P., Jeevanantham, V., & Saravanan, R. Archives of Metallurgy and Materials, *66*(3), (2021): 911-915. DOI: 10.24425/amm.2021.136397

[5] Nikitin, Aleksey A., Anna V. Ivanova, Alevtina S. Semkina, Polina A. Lazareva, Maxim A. Abakumov, International Journal of Molecular Sciences 23, no. 19 (2022): 11134; https://doi.org/10.3390/ijms231911134

[6] Li, Wei, Hanchen Tian, Liang Ma, Yi Wang, Xingbo Liu, Xuefei Gao, Materials Advances 3, no. 14 (2022): 5598-5644; https://doi.org/10.1039/D2MA00185C

[7] Bandyopadhyay, A., B. J. Sarkar, S. Sutradhar, J. Mandal, P. K. Chakrabarti, Journal of Alloys and Compounds 865 (2021): 158838; https://doi.org/10.1016/j.jallcom.2021.158838

[8] Bhuvaneshwari, S., Satheeskumar, S., Velayutham, J., & Rahman, B. S. Rasayan J. Chem, 14, (2021); 1581-1586. http://doi.org/10.31788/ RJC.2021.1436022

[9] Chong, Wei Juene, Shirley Shen, Yuncang Li, Adrian Trinchi, Dejana Pejak, Ilias Louis Kyratzis, Antonella Sola, Cuie Wen, Journal of Materials Science & Technology 111 (2022): 120-151; https://doi.org/10.1016/j.jmst.2021.09.039

[10] Shakila, P. B., Jeevanantham, V., Nagalakshmi, R., & Saravanan, R. (2023). Biomass Conversion and Biorefinery, 1-11. https://doi.org/10.1007/s13399-023-04793-7

[11] Maru, Apexa, C. M. Panchasara, K. N. Rathod, Hetal Boricha, Khushal Sagapariya, Bhagyashree Udeshi, Ajay Vaishnani et al., Bulletin of Materials Science 46, no. 3 (2023): 150; https://doi.org/10.1007/s12034-023-02985-5

[12] Gopinatha, P., Suresh, P., & Jeevanantham, V. Journal of Ovonic Research, 19, No 1, (2023) 23-30 https://doi.org/10.15251/JOR.2023.191.23

[13] Carofiglio, Marco, Marco Laurenti, Veronica Vighetto, Luisa Racca, Sugata Barui, Nadia Garino, Roberto Gerbaldo, Francesco Laviano, Valentina Cauda, Nanomaterials 11, no. 10 (2021): 2628; https://doi.org/10.3390/nano11102628

[14] Yu, Meng, Fangming Liu, Jinhan Li, Jiuding Liu, Yudong Zhang, Fangyi Cheng, Advanced Energy Materials 12, no. 4 (2022): 2100640; https://doi.org/10.1002/aenm.202100640

[15] Sahu, Dojalisa, Amrita Palai, Nihar Ranjan Panda, ECS Journal of Solid State Science and Technology (2023).

[16] Jeevanantham, V., Tamilselvi, D., Rathidevi, K., Bavaji, S. R., & Neelakandan, P. Biomass Conversion and Biorefinery, (2023):1-10. https://doi.org/10.1007/s13399-023-04179-9